International Journal of Multiphase Flow 85 (2016) 110–122

Contents lists available at ScienceDirect

International Journal of Multiphase Flow

journal homepage: www.elsevier.com/locate/ijmultiphaseflow

Interfacial area transport across a 90° vertical-upward elbow in air–water bubbly two-phase flow

Shouxu Qiao, Seungjin Kim*

230 Reber Building, Department of Mechanical and Nuclear Engineering, The Pennsylvania State University, University Park, PA 16802, USA

ARTICLE INFO

Article history:
Received 14 March 2016
Revised 15 May 2016
Accepted 31 May 2016
Available online 8 June 2016

Keywords:
Interfacial area transport
One-group
Elbow effect
Dissipation length
Bubbly flow

ABSTRACT

This study develops a one-group interfacial area transport equation (IATE) for vertical-upward-to-horizontal air–water bubbly two-phase flows through a 90° elbow with a non-dimensional centerline radius of curvature of three. In order to develop the model, an extensive database is established by acquiring local two-phase flow parameters using a four-sensor conductivity probe upstream and downstream of the elbow. The data show there exist three characteristic regions in void distribution, including a bimodal-to-bimodal region, a bimodal-to-single-peaked region, and a developed horizontal flow region with void accumulated at the top of the pipe cross-section. Using the database, the preliminary dissipation length model developed by Yadav et al. (2014b) is improved by including the transition region near the exit of the elbow in addition to the dissipation region. To close the IATE model, the bubble velocity advection term and bubble interaction terms in the IATE are correlated with the parameter characterizing the "*elbow-strength*". The two-phase pressure drop across the elbow is modeled using the modified Lockhart–Martinelli correlation which takes into account the minor loss effect. The closed IATE model is implemented to predict interfacial area transport in vertical-upward-to-horizontal two-phase flow. It is found that the developed model is capable of predicting interfacial area concentration with an average percent difference of less than ±6%.

© 2016 Elsevier Ltd. All rights reserved.

1. Introduction

In the study of two-phase flow, empirical correlations and models are often developed using the experimental data acquired in a test section with fixed orientation and with no flow restrictions. For example, the interfacial area transport equation (IATE), which predicts interfacial area concentration dynamically by modeling of various mechanisms that change the interfacial structure, has been developed for vertical and horizontal orientations (Ishii et al., 2002, 2004; Talley, 2012), but with no flow restrictions. In practical systems, a variety of flow restrictions such as elbows, valves, tees, nozzles and diffusers usually exist. The presence of flow restrictions can significantly affect both global and local two-phase flow parameters including flow regime transition, pressure drop, advection, phase distribution, and particle interaction mechanisms (Salcudean et al., 1983; Wang et al., 2004). For example, the spacer grid can promote bubble coalescence or break up depending on the flow regimes transitions (Wheeler et al., 2014). Different types of inlets also show significant effects on flow regime transition, pressure drop and development of the local two-phase flow parameters in vertical-downward two-phase flow (Qiao et al., 2016). Therefore, experimental and theoretical studies of flow restriction effects on two-phase flow are of significant importance.

Among the limited studies available concerning the effect of flow restrictions on interfacial structures, Kim et al. (2007) and Talley et al. (2009) investigated the effects of 90° and 45° horizontal elbows, respectively, on local two-phase flow parameters and their transport characteristics in air–water bubbly flow. These studies demonstrate that elbows induce distortions in the local void fraction profiles, which dissipate further downstream of the elbow. Moreover, it was shown that depending on the flow condition, the elbows promote either bubble coalescence or bubble breakup, which leads to significant changes in the interfacial area concentration.

Yadav et al. (2014a, b) investigated the geometric effects of a 90° vertical-upward elbow on advection of bubble velocity, void fraction distribution, and interfacial area concentration transport across the elbow in air–water two-phase flow. They found that bubbles moving through a vertical-upward elbow are entrained by the secondary flow leading to a bimodal distribution in bubbly flow conditions. This bimodal distribution then dissipates to single-peaked distribution near the top of the pipe as the flow develops downstream. To quantify the dissipation characteristics, the *elbow-strength* (S) is defined as the inverse of the second moment of the local void fraction distribution. A preliminary "Dissipation length

* Corresponding author. Fax: +1 814 863 4848.
E-mail address: skim@psu.edu (S. Kim).

http://dx.doi.org/10.1016/j.ijmultiphaseflow.2016.05.015
0301-9322/© 2016 Elsevier Ltd. All rights reserved.

model" was developed using *elbow-strength* to quantify the length of the region affected by the elbow. However, the model neglects the initial increasing trend of *elbow-strength* and assumes it decreases exponentially with increasing development length in the elbow-region due to the limitations of the database.

Currently, there are insufficient experimental database and models for predicting two-phase flow in the elbow region. This may limit the application of IATE models that are developed for vertical and horizontal orientations when flow restrictions exist. In order to bridge the transition between the vertical and horizontal orientations, it is important to understand the geometric effects of elbows on both global and local two-phase flow parameters. In addition, the development and benchmarking of multiphase flow computational fluid dynamics codes (CFD) requires an experimental database of detailed local measurements (Lucas et al., 2010). In view of this, the objectives of the current study are: (1) to perform two-phase flow experiments to establish additional database for local and global two-phase flow parameters downstream of a vertical-to-horizontal elbow, (2) to improve the preliminary "Dissipation length model" by Yadav et al. (2014b) by including the transition trend of *elbow-strength* in the elbow region, (3) to develop a steady-state one-group IATE applicable to the elbow region, and (4) to implement and evaluate the developed steady-state one-group IATE in vertical-upward-to-horizontal bubbly flow.

2. Experimental studies

This section describes the experimental study that is performed to investigate the effects of a 90° vertical-upward elbow on local two-phase flow parameters in air–water bubbly two-phase flow. The experiments are performed by taking local two-phase flow data near the exit of the elbow in addition to the existing database developed by Yadav et al. (2014a). The experimental results are discussed to show the geometric effects of the elbow on the two-phase flow parameters, which are crucial towards the development of the IATE for the elbow-region.

2.1. Experimental setup and test conditions

The schematic diagram of the test facility is shown in Fig. 1. The test section is constructed from 5.08 cm inner-diameter (D) acrylic pipe segments that are arranged in a loop configuration with three vertical and two horizontal sections. The vertical and horizontal sections are interconnected by four 90° glass elbows, which have a non-dimensional radius of curvature, R_C/D, of three. The lengths of the vertical and horizontal sections are 3.35 m and 9.45 m, which yield development lengths of *66D* and *186D*, respectively. The multiple vertical and horizontal sections allow for investigation of all conceivable vertical-to-horizontal and horizontal-to-vertical two-phase flow configurations connected by 90° vertical elbows. For the present study, co-current vertical-upward air–water two-phase flow is introduced at inlet A via a two-phase flow injection system, which is designed to provide a uniform inlet bubble size of approximately 2–3 mm. Additional details about the experimental facility are provided in Yadav et al. (2014a).

Yadav et al. (2014a) developed a detailed database for two-phase flow from vertical-upward through a 90° vertical-elbow to horizontal two-phase flow. With the database, they were able to quantify the elbow region by characterizing the variation of the void distribution downstream of the vertical-upward elbow. However, the database lacks data at the exit of the elbow, $L/D]_H = 0$. Data here are important because they provide the initial flow condition after the elbow and can be used to normalize the data downstream. In the modeling of the IATE, the *elbow-strength* parameter, the area-averaged void-weighted bubble velocity, and the bubble distribution parameters have to be normalized to their values at $L/D]_H = 0$. In view of this, the present study performs two-phase flow measurements at $L/D]_H = 0$ for all flow conditions. In addition, two-phase flow measurements are also performed at $L/D]_H = 9$ for Run7 and Run8 to provide more detailed parameter values of the two-phase flow downstream of the elbow for $j_f = 4.00$ m/s. The new test conditions are indicated by √ marks in Table 1.

Table 1
Summary of test conditions and axial measurement locations in the horizontal section (X and √ denote axial measurement locations).

Run #	$j_{g,atm}$ [m/s]	j_f [m/s]	Horizontal section, $L/D]_H$ [dimensionless] 0	3	9	21	33	63	93	177
Run1	0.13	2.00	√	X			X		X	X
Run2	0.23	2.00	√	X	X	X	X		X	X
Run3	0.34	2.00	√	X	X		X		X	X
Run4	0.14	3.00	√	X	X		X		X	X
Run5	0.23	3.00	√	X	X	X	X		X	X
Run6	0.35	3.00	√	X	X	X	X		X	X
Run7	0.23	4.00	√	X	√	X	X	X	X	X
Run8	0.35	4.00	√	X	√	X	X	X	X	X

In Table 1, $L/D]_H$ denotes the non-dimensional distance from the exit of the vertical-upward elbow in the horizontal section to the axial measurement location. The flow conditions are specified by their liquid superficial velocity (j_f), and gas superficial velocity ($j_{g,atm}$). The subscript *atm* indicates that the gas superficial velocities shown are evaluated at the atmospheric pressure condition.

The flow conditions are selected to be within the bubbly flow regime in the vertical-upward section. At each axial measurement location, the state-of-the-art four sensor conductivity probe (Kim et al., 2000) is used to measure local time-averaged two-phase flow parameters including the void fraction (α), bubble frequency (f_b), bubble velocity (v_g), and interfacial area concentration (a_i), at multiple points within the flow cross-section. The measurement principle of the multi-sensor conductivity probe in obtaining local time-averaged a_i is based on the definition given by Ishii (1975), where the local time-averaged a_i is defined by Kataoka et al. (1986):

$$\overline{a_i}^t = \frac{1}{\Delta T}\sum_j \left(\frac{1}{|\boldsymbol{v_i}\cdot\boldsymbol{n_i}|}\right)_j \tag{1}$$

where, the subscript j denotes the jth interface which passes a local point during the time interval, ΔT. $\boldsymbol{v_i}$ and $\boldsymbol{n_i}$ are the bubble interfacial velocity and unit surface normal vector of the jth interface, which can be determined from the probe measurement and probe configuration.

At each measurement point, the data acquisition time is varied to obtain a minimum sample size of 2000 bubbles such that the statistical error is within ±7% (Wu and Ishii, 1999). Since bubble distribution in the horizontal section is inherently asymmetric due to buoyancy, local conductivity probe measurements are performed throughout the entire pipe cross-section. This is achieved by installing the probe using a specialized instrumentation port that can be rotated around the axis of the pipe in 22.5° intervals in the azimuthal direction, which allows for data acquisition without stopping the flow. Fig. 2 shows the measurement mesh used for horizontal two-phase flow data measurement. In the figure, the flow direction is out of the page and the non-dimensional radial distance along an azimuthal angle is denoted by $(r/R)_\theta$. Therefore, $(r/R)_0$ and $(r/R)_{90}$ correspond to the horizontal and vertical axis of the pipe cross-section, respectively, with respect to the direction of gravity. Along each azimuthal direction, the probe is traversed along a single diameter in the cross-section to obtain local measurements at the following radial positions: $(r/R) = 0.0, \pm 0.2, \pm 0.4,$

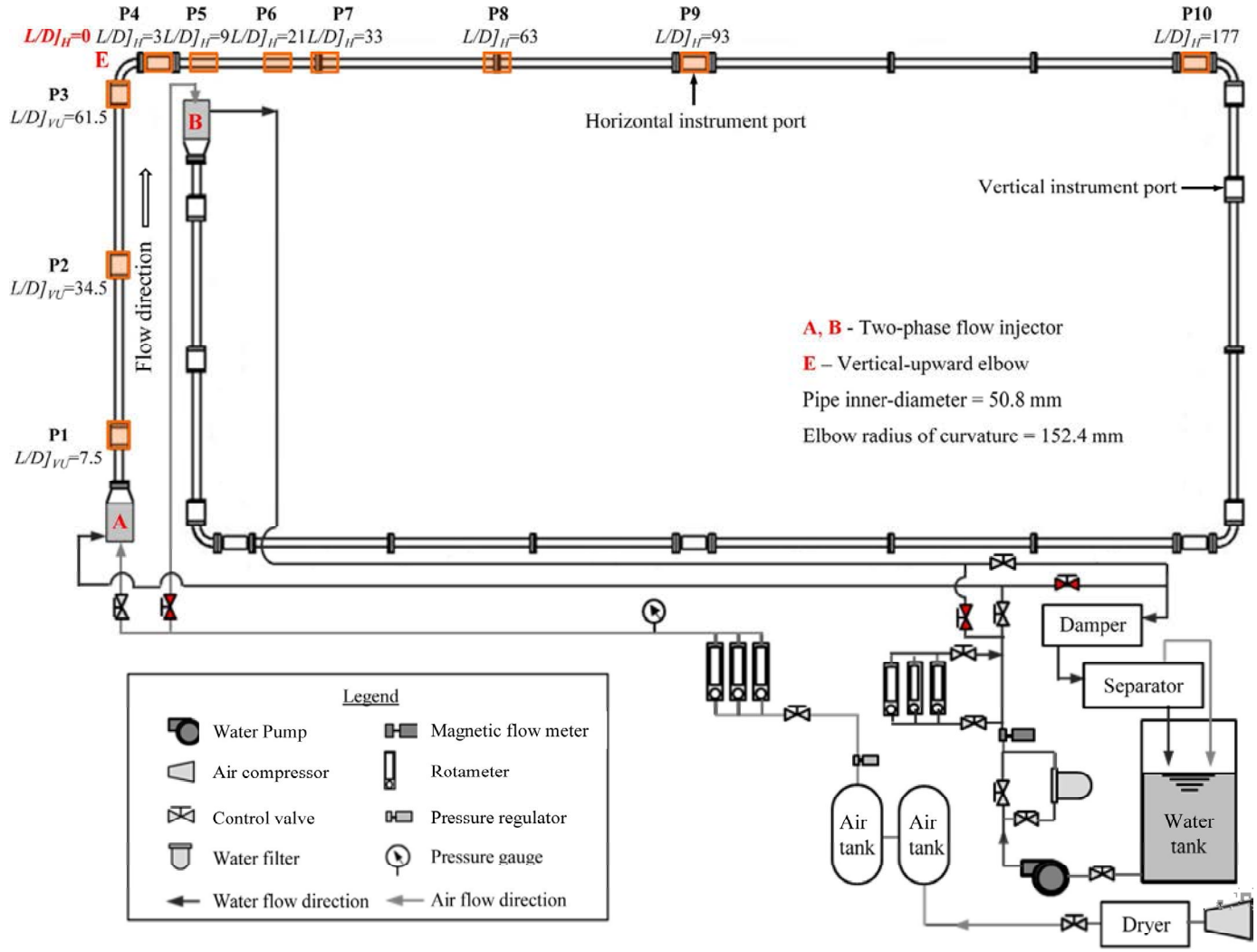

Fig. 1. Simplified schematic diagram of the test facility. For the current experiments, injector A is used as the inlet and injector B is used as the outlet.

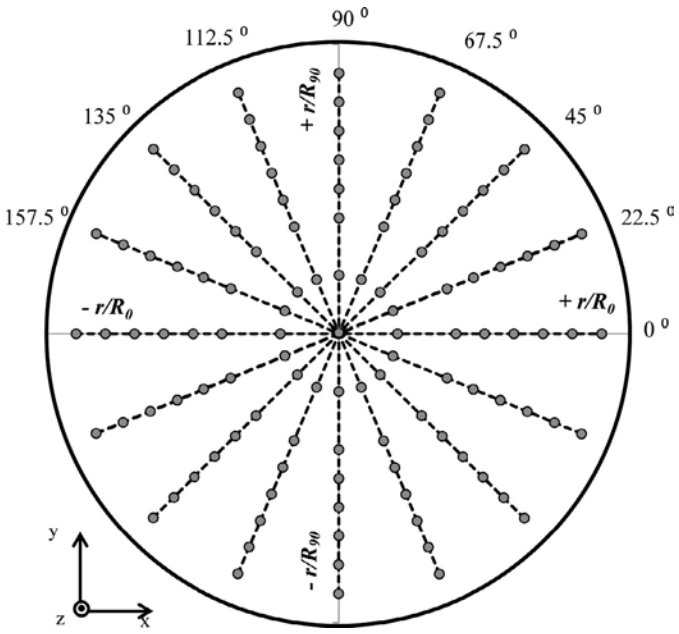

Fig. 2. Measurement mesh used to measure local two-phase flow parameters.

±0.5, ±0.6, ±0.7, ±0.8, and ±0.9. Here, r/R is the non-dimensional radial coordinate, and R is the inner radius of the pipe. Hence, a total of 120 local data points, are measured across the entire pipe cross-section.

2.2. Experimental results

Fig. 3 shows the surface plots of the measured local void fraction and a_i obtained with the conductivity probe at $L/D]_H=0$ for Run4. Similar to the void fraction distribution observed by Yadav et al. (2014b) at $L/D]_H=3$, the void fraction distribution at $L/D]_H=0$ also shows a "bimodal-type" distribution. However, the void fraction peaks are located closer to the bottom of the horizontal pipe, or near $(r/R)_{90}=-0.4$ at $L/D]_H=0$. This is different from the distribution at $L/D]_H=3$ where the void fraction peaks are approximately at the center of the pipe or $(r/R)_{90}=0$. This is because the liquid phase velocity along the outer curvature of the elbow is larger than that along the inner curvature when two-phase flow crosses the elbow. The larger liquid phase velocity along the outer curvature will force bubbles to migrate towards the inner curvature of the elbow and accumulate near the bottom of the elbow exit. For a_i, a similar "bimodal-type" distribution is observed due to the linear relationship between void fraction and a_i in the bubbly flow regime.

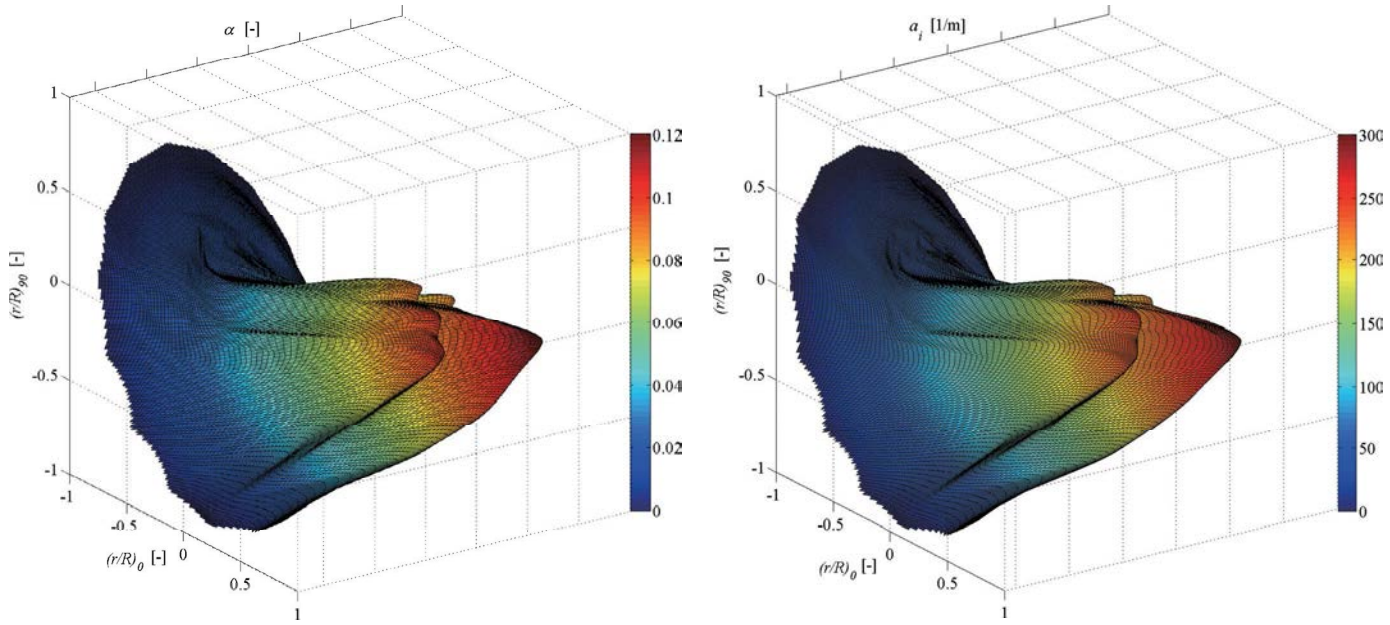

(a) void fraction, α (b) interfacial area concentration, a_i

Fig. 3. Surface plots of measured (a) α and (b) a_i at $L/D|_H = 0$ for Run4 ($j_f = 3.00$ m/s and $j_{g,atm} = 0.14$ m/s).

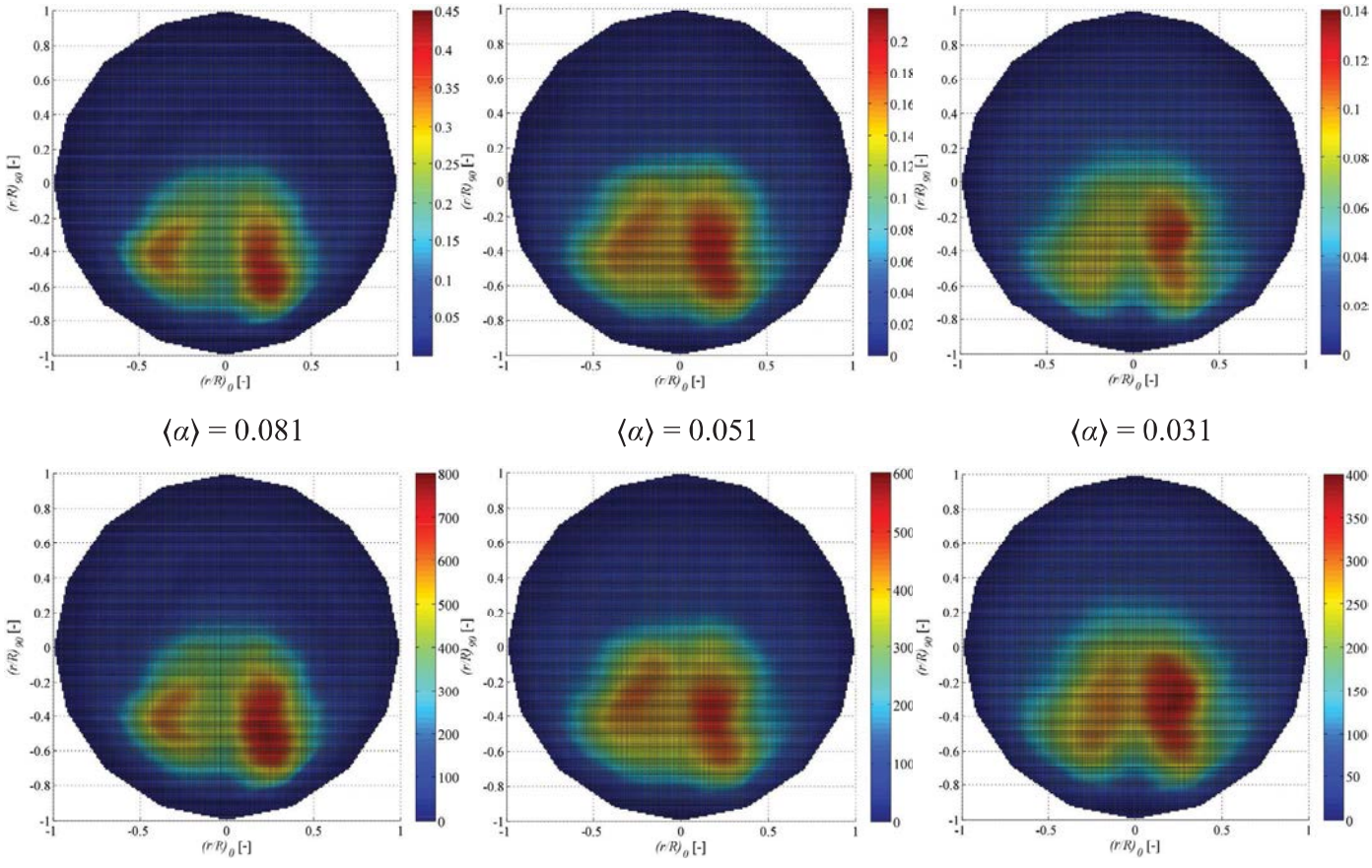

$\langle\alpha\rangle = 0.081$ $\langle\alpha\rangle = 0.051$ $\langle\alpha\rangle = 0.031$

$\langle a_i\rangle = 156$ [1/m] $\langle a_i\rangle = 138$ [1/m] $\langle a_i\rangle = 102$ [1/m]

(a) Run2 ($j_f = 2.00$ m/s) (b) Run5 ($j_f = 3.00$ m/s) (c) Run7 ($j_f = 4.00$ m/s)

Fig. 4. Contour plots of measured α and a_i for (a) Run2, (b) Run5, and (c) Run7 at $L/D|_H = 0$ ($j_{g,atm} = 0.23$ m/s).

freepaper.me FREE paper

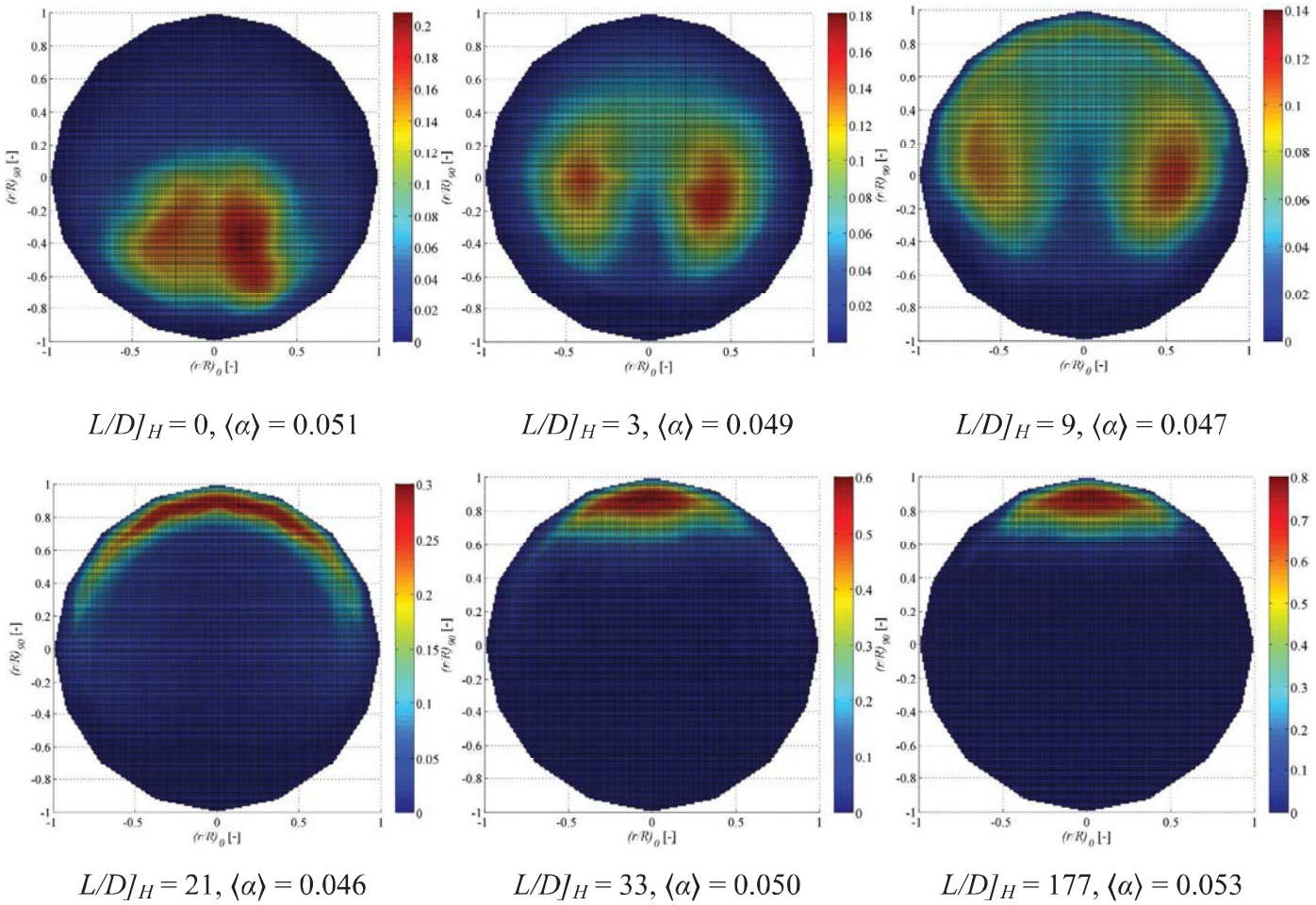

Fig. 5. Axial development of measured α for Run5 ($j_f = 3.00$ m/s and $j_{g,atm} = 0.23$ m/s).

Fig. 4(a)–(c) shows the contour plots of the measured void fraction and a_i at $L/D]_H = 0$ for Run2, Run5, and Run7, respectively. For $j_f = 2.00$ m/s (Run2), it is observed that the void fraction shows a bimodal-type distribution and the peaks occur near the center of the bottom half of the pipe, or $(r/R)_{90} \approx -0.4$. Similar void fraction distribution characteristics are observed when increasing j_f from 2.00 m/s to 3.00 m/s (Run5) and 4.00 m/s (Run7). For a_i, the peaks also occur at a similar height, or $(r/R)_{90} \approx -0.4$. This indicates the bubble distribution at the exit of the elbow is governed by inertia, and buoyancy is not strong enough to push the bubbles upwards.

Figs. 5 and 6 show the axial development of the measured void fraction and a_i from the exit of elbow, $L/D]_H = 0$, to the end of the horizontal section, $L/D]_H = 177$, for Run5. It is observed that the distributions of void fraction and a_i show three distinctive regions, i.e., (a) bimodal-to-bimodal distribution between $L/D]_H = 0$ and 9, (b) bimodal-to-single-peaked distribution between $L/D]_H = 9$ and 21, and (c) developed horizontal flow between $L/D]_H = 21$ and 177. One may notice that the distributions of the local void fraction and a_i are not completely symmetric and consistently higher on the positive side of $(r/R)_0$. Ideally, the distributions of the time-averaged two-phase flow parameters under steady-state conditions should be symmetric about the $(r/R)_0 = 0$ line at different axial locations. The asymmetry in the data, however, can be caused presumably by (a) degree of steadiness of the two-phase flow and (b) any slight misalignment between the 90° elbow and the vertical or horizontal pipe sections. To reduce such effects, great efforts were made (a) in maintaining the flow rates constant throughout the experiments and (b) in aligning the test sections as best as possible by employing different methods.

3. Model development

This section presents the development and assessment of the one-group IATE model for the elbow region. The "Dissipation length model" developed by Yadav et al. (2014b) is modified by modeling the transition region near the exit of the elbow. The bubble velocity advection term and bubble interaction terms in the IATE are correlated with the *elbow-strength*. The two-phase pressure drop across the elbow is modeled using the modified Lockhart–Martinelli correlation by Kim et al. (2010). The developed IATE is then implemented to predict interfacial area transport in the vertical-upward-to-horizontal two-phase flow.

3.1. Predictive model development

The steady-state, one-dimensional, one-group IATE is given as (Kim, 1999):

$$\langle a_i \rangle \frac{d\langle\langle v_g \rangle\rangle}{dz} + \langle\langle v_g \rangle\rangle \frac{d\langle a_i \rangle}{dz} = \frac{2}{3}\left(\frac{\langle a_i \rangle \langle\langle v_g \rangle\rangle}{p}\right)\left(-\frac{dp}{dz}\right) + \langle \phi_{RC} \rangle + \langle \phi_{TI} \rangle + \langle \phi_{WE} \rangle \quad (2)$$

In Eq. (2), z, p, and ϕ denote the axial length, the local pressure, and the source or sink to a_i, respectively. The terms on the left hand side represent the advection of a_i. The first

دانلود کننده مقالات علمی freepaper.me FREE paper

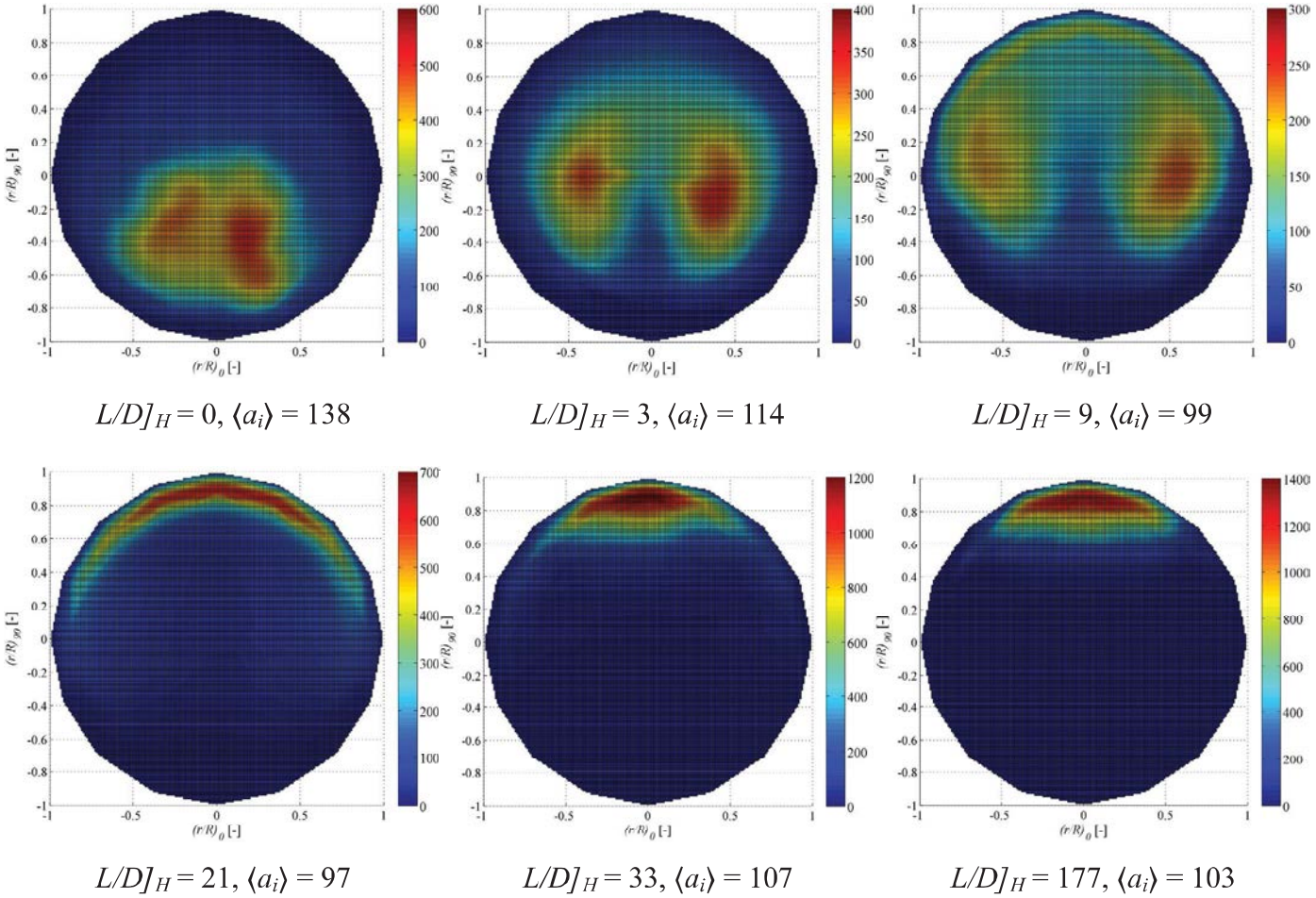

Fig. 6. Axial development of measured a_i for Run5 ($j_f = 3.00$ m/s and $j_{g,atm} = 0.23$ m/s).

term on the right hand side represents the change in a_i due to the compressibility of the dispersed phase while the remaining three terms represent the change in a_i due to the random collision of bubbles driven by the turbulent eddies in the continuous phase (*RC*), the impact of turbulent eddies in the continuous phase (*TI*), and the coalescence of bubbles due to wake entrainment (*WE*), respectively. Modeling of these terms requires information about the local two-phase flow parameters, which is generally not available during a one-dimensional analysis. In flow conditions with almost uniformly distributed local two-phase flow parameters (for example, dispersed bubbly flow in vertical configuration), the area-averaged value of the two-phase flow parameters can be employed to calculate the source/sink terms. However, this approach is not valid in the present flow conditions with highly skewed distribution of local two-phase flow parameters because asymmetric distributions lead to non-unity covariance among different two-phase flow parameters (Hibiki and Ishii, 2000). In order to evaluate area-averaged source/sink terms due to bubble interactions, a covariance-type term is introduced such that, for any two parameters a and b, it is defined as:

$$COV(a,b) = \frac{\langle ab\rangle}{\langle a\rangle\langle b\rangle} \tag{3}$$

This covariance term exists because the area-average of the product of two or more parameters is not the same as the product of the area averages of the parameters. It should be noted that *COV(a, b)* becomes unity in case of flows with uniform profiles and it changes continuously with the change in distribution of a and/or b. In two-phase flow downstream of the elbow, however, the covariance terms in the bubble interaction mechanisms need to be modeled. In the current study, they are modeled as (Talley, 2012; Yadav, 2013):

$$\langle \phi_{TI}\rangle = COV_{TI} C_{TI} \frac{1}{18}\frac{\langle a_i\rangle^2}{\langle\alpha\rangle}\langle v_t\rangle\sqrt{1-\frac{We_{cr}}{We}}\exp\left(-\frac{We_{cr}}{We}\right) \quad for\, We > We_{cr} \tag{4}$$

$$\langle \phi_{RC}\rangle = -COV_{RC} C_{RC}\frac{1}{3\pi}\frac{\langle a_i\rangle^2\langle v_t\rangle}{\alpha_{max}^{1/3}\left(\alpha_{max}^{1/3}-\langle\alpha\rangle^{1/3}\right)}\left[1-\exp\left(-C\frac{\alpha_{\max}^{1/3}\langle\alpha\rangle^{1/3}}{\alpha_{\max}^{1/3}-\langle\alpha\rangle^{1/3}}\right)\right] \tag{5}$$

$$\langle \phi_{WE}\rangle = -COV_{WE} C_{WE}\frac{1}{3\pi}C_D^{1/3}\langle a_i\rangle^2\langle v_t\rangle \tag{6}$$

where, the covariance terms can be calculated as following:

$$COV_{TI} = \frac{\left\langle \frac{a_i^2}{\alpha} v_t\sqrt{1-\frac{We_{cr}}{We}}\exp\left(-\frac{We_{cr}}{We}\right)\right\rangle}{\frac{\langle a_i\rangle^2}{\langle\alpha\rangle}\langle v_t\rangle\sqrt{1-\frac{We_{cr}}{\langle We\rangle}}\exp\left(-\frac{We_{cr}}{\langle We\rangle}\right)} \tag{7}$$

$$COV_{RC} = \frac{\left\langle \frac{a_i^2 v_t}{\alpha_{\max}^{1/3}-\alpha^{1/3}}\left[1-\exp\left(-C\frac{\alpha_{\max}^{1/3}\alpha^{1/3}}{\alpha_{\max}^{1/3}-\alpha^{1/3}}\right)\right]\right\rangle}{\frac{\langle a_i\rangle^2\langle v_t\rangle}{\alpha_{\max}^{1/3}-\langle\alpha\rangle^{1/3}}\left(1-\exp\left(-C\frac{\alpha_{\max}^{1/3}\langle\alpha\rangle^{1/3}}{\alpha_{\max}^{1/3}-\langle\alpha\rangle^{1/3}}\right)\right)} \tag{8}$$

$$COV_{WE} = \frac{\langle a_i^2 v_t \rangle}{\langle a_i \rangle^2 \langle v_t \rangle} \tag{9}$$

In equations above, C, C_{TI}, C_{RC}, and C_{WE} are empirical coefficients; v_t, We, and C_D are the *rms* turbulent velocity fluctuation in the liquid phase, the particle Weber number, and the particle drag coefficient, respectively. We_{cr} denotes the critical Weber number below which the turbulent eddies cannot breakup bubbles and α_{max} denotes the maximum void fraction when bubbles approach the dense packing limit (Wu et al., 1998). The $\langle\ \rangle$ and $\langle\langle\ \rangle\rangle$ brackets represent area-averaged and void-weighted area-averaged quantities, respectively.

To model a_i transport from vertical-upward-to-horizontal two-phase flow, three separate regions, i.e., (1) vertical-upward, (2) elbow, and (3) horizontal section are considered (Yadav, 2013). In the vertical-upward and horizontal section, IATEs developed by Ishii et al. (2002) and Talley (2012) can be applied, respectively. In the elbow region, Yadav's (2013) model can be applied. The current study focuses on improving the IATE model applicable to the elbow region established by Yadav's (2013) to provide more accurate predictions of a_i between vertical-upward and horizontal sections. As such, the flow at the exit of the vertical-upward section provides the inlet boundary conditions for the elbow region and the flow at the exit of the elbow region provides the inlet boundary conditions for the horizontal section.

In order to develop an IATE which is applicable to the elbow region, the length of the elbow region, the void-weighted area-averaged gas velocity term, and the a_i source and sink terms have to be modeled. These include:

(a) The dissipation length which defines the region to implement the IATE model;
(b) The void-weighted area-averaged gas velocity, $\langle\langle v_g \rangle\rangle$, which describes the advection of a_i in the IATE;
(c) The covariance in the bubble interaction terms, $\langle\phi\rangle_{RC}$, $\langle\phi\rangle_{TI}$, and $\langle\phi\rangle_{WE}$, which are sources/sinks to a_i in the IATE;
(d) Two-phase pressure drop across the elbow, $-\partial p/\partial z$, which is also source/sink to a_i in the IATE.

3.2.1. Modeling of the elbow dissipation length

To quantify the dissipation length or the length of the region affected by the elbow, Yadav et al. (2014b) defines the *elbow-strength* (S) as:

$$S \equiv \frac{1}{\sigma}, \text{ where, } \sigma \equiv \frac{1}{A}\int \frac{(\alpha - \langle\alpha\rangle)^2}{\langle\alpha\rangle^2} dA \tag{10}$$

In Eq. (10), σ is the second moment of the void fraction, which physically describes the variance of the void distribution. σ approaches to zero for a uniform distribution. In the region downstream of the elbow, σ increases as the flow develops because the void distribution becomes more skewed as bubbles start to migrate toward the top of the pipe. S is defined as the reciprocal of σ so that it decreases as the flow develops. According to Yadav et al. (2014b), the void distributions for Run4–Run8 (j_f=3.00 and 4.00 m/s conditions) have three distinct regions, i.e., (a) bimodal-to-bimodal distribution, (b) bimodal-to-single-peaked distribution, and (c) developed horizontal flow as shown in Fig. 5. Accordingly, S increases in region (a), decreases in region (b), and remains close to constant in region (c). However, data for region (a) is not available in the database by Yadav et al. (2014a) for Run1–Run3 (j_f=2.00 m/s conditions). To develop a universal model for S, region (a) in Run4–Run8 is neglected such that S shows a decreasing trend for all runs in their modeling. This simplification may induce errors in a_i modeling. With the new experimental data acquired at $L/D]_H$=0, experimental results in Section 2.2 show that region (a) also exists for j_f=2.00 m/s conditions and therefore the transition

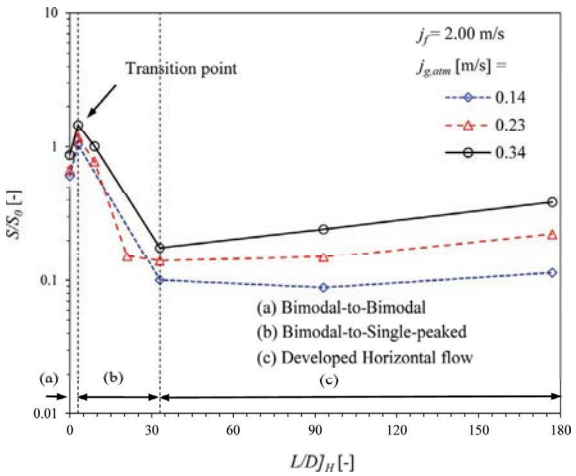

(a) j_f = 2.00 m/s

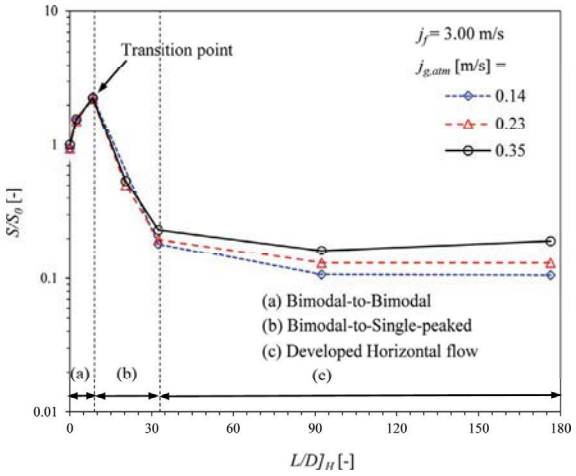

(b) j_f = 3.00 m/s

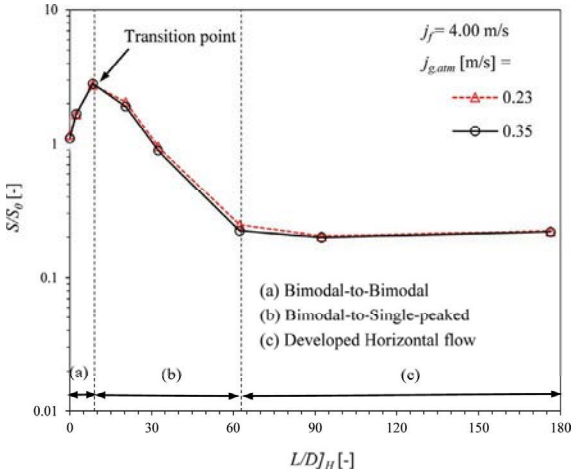

(c) j_f = 4.00 m/s

Fig. 7. Evolution of S along the axial direction downstream of the elbow for (a) j_f=2.00 m/s, (b) j_f=3.00 m/s, and (c) j_f=4.00 m/s.

freepaper.me FREE paper

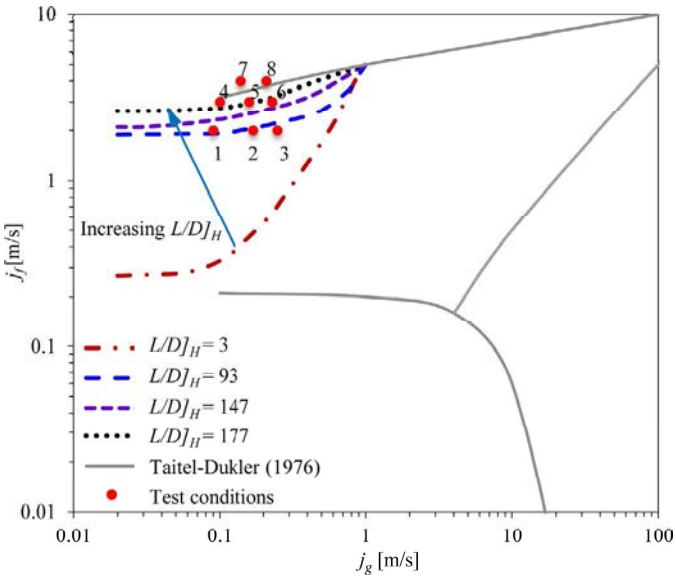

Fig. 8. Flow conditions shown on the horizontal flow regime map (j_g measured at $L/D]_H$ =177). The reference cite in this figure Taitel and Duckler (1976).

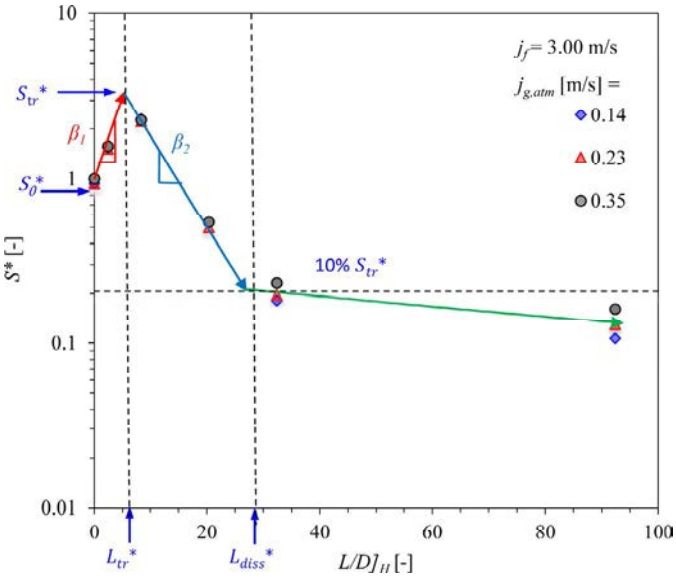

Fig. 9. Characterization of the elbow-strength for j_f=3.00 m/s.

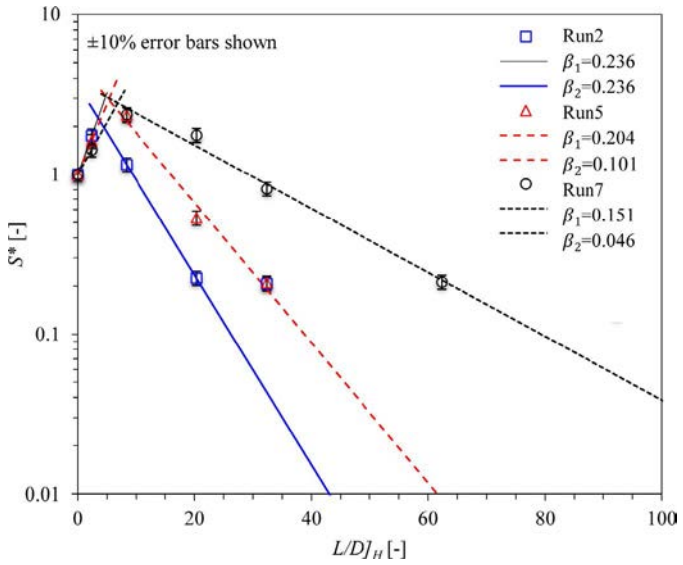

Fig. 10. Fitting of β_1 and β_2 to experimental data for Run2, Run5, and Run7.

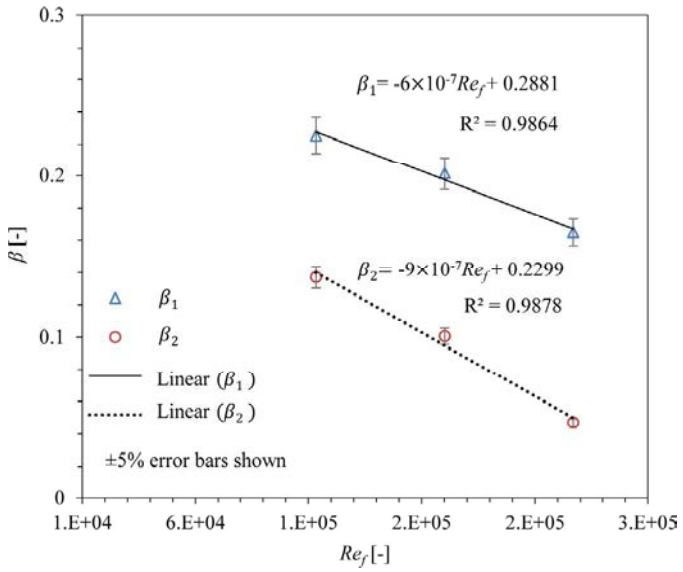

Fig. 11. Correlation of β_1 and β_2 with Re_f.

region for all flow conditions can be modeled with greater precision. Fig. 7(a)–(c) plots the evolution of S along the axial direction downstream of the elbow which show the increasing to decreasing trend of S for different flow conditions. From the figures, the evolution of S for all flow conditions shows similar characteristics and can be separated into three regions:

(a) Transition region – bimodal-to-bimodal, S increases;
(b) Dissipation region – bimodal-to-single-peaked, S decreases;
(c) Asymptotic region – developed horizontal flow, S remains close to constant.

From Fig. 7, one may notice that S increases slightly with $L/D]_H$ for j_f=2 m/s conditions while it remains almost truly constant for j_f=3 and 4 m/s conditions. This is believed to be caused by the change of flow regimes as two-phase flow develops in the horizontal section. Fig. 8 shows the eight experimental conditions on a modified horizontal two-phase flow regime map by Yadav (2013). In the figure, different dotted lines denote the transition from bubbly flow to intermittent flow (plug flow or slug flow) at different development length. As can be seen, Run4, Run7, and Run8 remain bubbly flow in the whole horizontal section. However, the flow regimes develop from bubbly flow to intermittent flow for Run1–Run3, Run5 and Run 6. In comparing the void distribution, intermittent flow is more uniform than bubbly flow and therefore the S parameter shows slight increase for j_f=2 m/s conditions.

To model the transition region, a methodology similar to that of Yadav et al. (2014b) is followed along with the following additional hypotheses:

(1) A transition point separates the elbow region into a transition region and a dissipation region;
(2) The evolution of S is an exponential function of the axial length $L/D]_H$, in both regions.

For the elbow region, the new dissipation length model is given by Eq. (11):

$$S^* = \begin{cases} \exp(\beta_1 L^*) & \text{for } 0 \le L^* \le L^*_{tr} \\ S^*_{tr} \exp[-\beta_2 (L^* - L^*_{tr})] & \text{for } L^*_{tr} < L^* \le L^*_{diss} \end{cases} \quad (11)$$

freepaper.me FREE paper

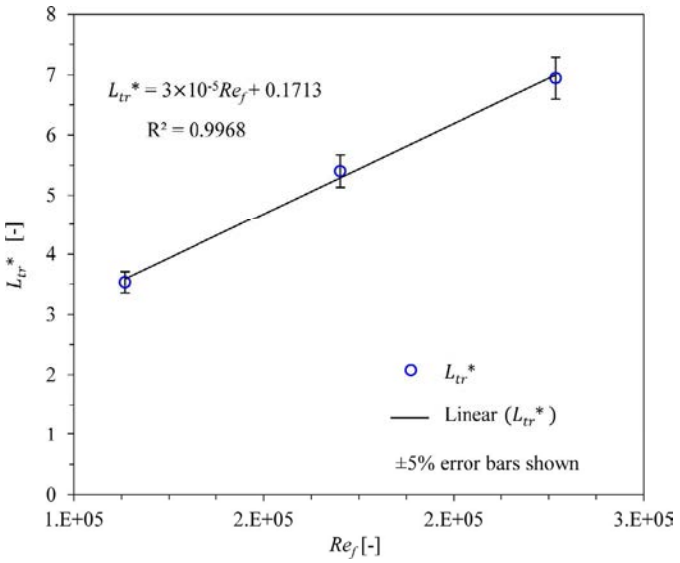

Fig. 12. Correlation of L_{tr}^* with Re_f.

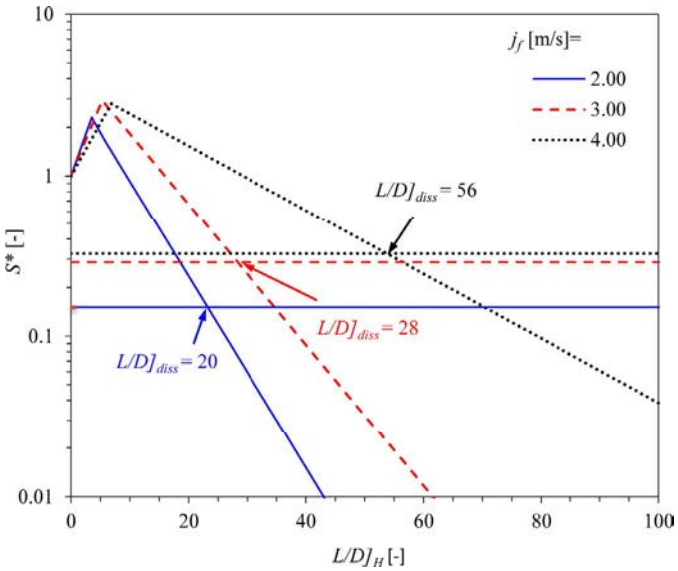

Fig. 13. Predicted dissipation length by the improve elbow-strength model.

All parameters in Eq. (11) are indicated in Fig. 9. Among them, $S^* = S/S_0$, S_{tr}^* is the value of S^* at the transition point. $L^* = L/D]_H$, L_{tr}^* and L_{diss}^* are the values of L^* at the transition point and dissipation point, respectively. β_1 and β_2 are the coefficients quantifying how quickly the transition and dissipation will happen; they can be determined from the slopes of the lines in the plot with a logarithmic y-axis.

To determine β_1, β_2, and L_{tr}^*, experimental data for Run2, Run5, and Run7 are fitted with Eqs. (12)–(14) as shown in Fig. 10. According to Yadav et al. (2014a) the dissipation of elbow-effects is a strong function of the liquid superficial velocity and a weak function of the gas superficial velocity within bubbly flow conditions. This is because the gas fraction (i.e., void fraction) is still too low to play significant role in determining the dissipation length such that most of bubbles are entrained by the liquid phase. As such, the inertia and centrifugal forces dominate the buoyancy force effect. Therefore, β_1, β_2, and L_{tr}^* are correlated with the liquid phase Reynolds number which is calculated using liquid properties and the pipe diameter as the characteristic length. Correlations for β_1, β_2, and L_{tr}^* are determined in Figs. 11 and 12 and shown below:

$$\beta_1 = -6\times10^{-7}\mathrm{Re}_f + 0.2881 \tag{12}$$

$$\beta_2 = -9\times10^{-7}\mathrm{Re}_f + 0.2299 \tag{13}$$

$$L_{tr}^* = 3\times10^{-5}\mathrm{Re}_f + 0.1713 \tag{14}$$

Following Yadav's modeling (Yadav et al., 2014b) for two-phase flow, the dissipation length of the elbow for different flow conditions in two-phase flow can be determined by defining a threshold value of S. In the present study, this threshold value is defined as 10% of the maximum value for each flow condition. In other words, the dissipation length in two-phase flow is the location where the normalized *elbow-strength* ($S*$) decreases to 10% of $S_{tr}*$. Based on the experimental data, the dissipation lengths are determined in Fig. 13.

A summary of model coefficients and dissipation parameters for all flow conditions are tabulated in Table 2. The last column in Table 2 summarizes the predicted dissipation length using the modified model. Overall, the dissipation lengths predicted by the current study are smaller than the predictions using the model by Yadav et al. (2014b). The precise modeling of the dissipation length is important because it determines the boundary for applying different IATE models and therefore will affect the prediction of the a_i and other parameters after the elbow.

3.2.2. Modeling of the advection term, $\langle\langle v_g\rangle\rangle$

From Eq. (2), the variation in $\langle a_i\rangle$ is closely related to the advection of bubble velocity $\langle\langle v_g\rangle\rangle$. Since $\langle\langle v_g\rangle\rangle$ is the void-weighted area-averaged bubble velocity which highlights the effect of change in bubble distribution, it is expected that the variation of $\langle\langle v_g\rangle\rangle$ can be correlated with S. Following this assumption, the axial evolution of the normalized $\langle\langle v_g\rangle\rangle$ is plotted together with the variation of normalized S versus $L/D]_H$ downstream of the elbow in Fig. 14. In the figure, both parameters are normalized by their values at the reference point $L/D]_H = 0$. $\langle\langle v_g\rangle\rangle/\langle\langle v_g\rangle\rangle_0$ is plotted on the primary y-axis with the linear scale, while S/S_0 is plotted on the secondary y-axis with the logarithmic scale. It is observed that both parameters show an increasing to decreasing trend. Therefore, a strong correlation between these two parameters is expected in the elbow region. In addition, it should be noted that similarity in the profiles is not a perfect comparison because $\langle\langle v_g\rangle\rangle$, in addition to bubble distribution, also weakly depends on the change in the velocity profile. The dependence on the velocity profile is neglected because its effect is small compared with that of the void distribution. Therefore, $\langle\langle v_g\rangle\rangle$ and S are correlated by the following equation:

$$\frac{\langle\langle v_g\rangle\rangle}{\langle\langle v_g\rangle\rangle_0} = 1 + C_{vg} ln\left(\frac{S}{S_0}\right) \tag{15}$$

where, the coefficient C_{vg} is a constant that is determined from the experimental data. By fitting the correlation with the experimental data as shown in Fig. 15, it is found that $C_{vg} = 0.09$ predicts the experimental data well for all flow conditions with an average percent difference of less than ±5%.

3.2.3. Modeling of the covariance in bubble interaction terms

Three covariance in bubble interaction terms, i.e., COV_{TI} COV_{RC}, and COV_{WE}, as shown in Eqs. (7)–(9) have to be modeled. The bubble collision term due to WE is neglected because the relative velocity between the two phases changes from positive to negative when the flow configuration changes from vertical-upward to horizontal. As such, the wake formation on the bubbles is opposite to the axial flow direction. Wake entrainment models the collision between two bubbles due to acceleration of a following bubble in

freepaper.me FREE paper

Table 2.
Summary of the dissipation parameters in the elbow-strength model for all flow conditions.

Run#	j_f [m/s]	Re_f [dimensionless]	β_1 [dimensionless]	β_2 [dimensionless]	L_{tr}* [dimensionless]	L_{diss}* [dimensionless]
Run1–Run3	2	101,397	0.226	0.137	3.5	20
Run4–Run6	3	152,095	0.201	0.101	5.4	28
Run7–Run8	4	202,794	0.165	0.047	6.9	56

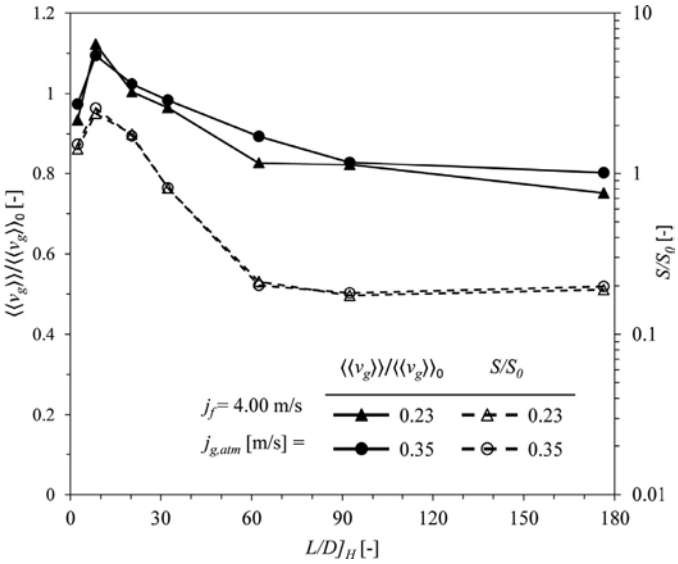

Fig. 14. Axial development of $\langle\langle v_g\rangle\rangle/\langle\langle v_g\rangle\rangle_0$ and S/S_0 in the downstream of the vertical-upward elbow for j_f=4.00 m/s and increasing $j_{g,atm}$.

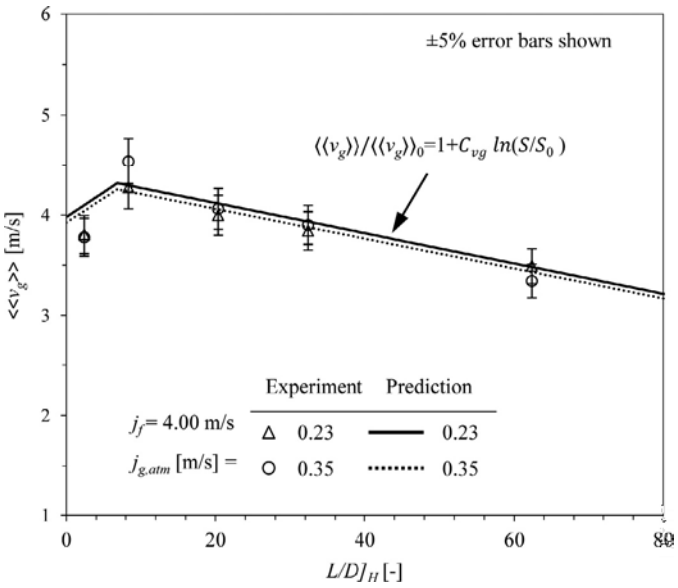

Fig. 15. Prediction of the $\langle\langle v_g\rangle\rangle$ in the downstream of the vertical-upward elbow for flow conditions with constant j_f=4.00 m/s and increasing $j_{g,atm}$.

the wake of the leading bubble. A change in the direction of the wake significantly reduces the acceleration between two bubbles leading to a reduced probability of collision. Therefore, the sink to $\langle a_i\rangle$ due to *WE*, COV_{WE}, is neglected in the elbow region and the horizontal section. For the other two terms, COV_{TI} is found to be negligible in the elbow region due to the fact that Weber number (*We*) remains below the critical Weber number (We_{cr}). Therefore, random collision is the only active bubble interaction mechanism in the elbow region.

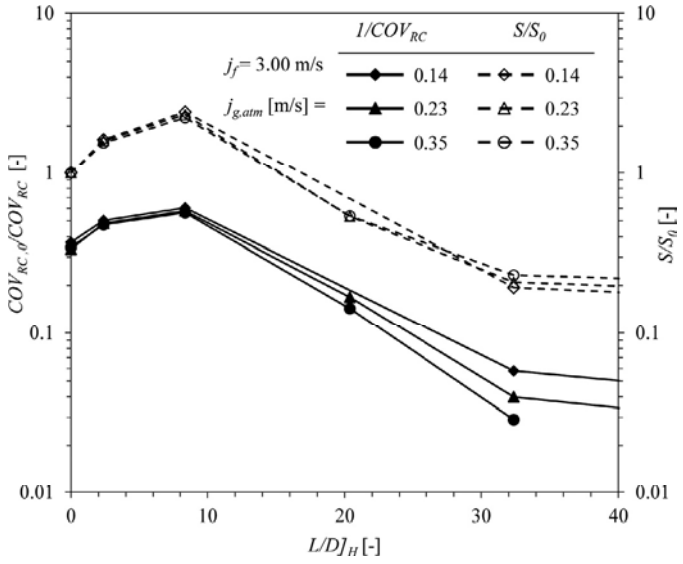

Fig. 16. Axial development of normalized $1/COV_{RC}$ and normalized *S* in the downstream of the vertical-upward elbow for j_f=3.00 m/s and increasing $j_{g,atm}$.

To develop a predictive model for the bubble distribution effect on the random collision sink term in the elbow region, a methodology similar to modeling of the advection of $\langle\langle v_g\rangle\rangle$ is applied. Since COV_{RC} describes the bubble distribution effects, it is expected that the variation of COV_{RC} can also be correlated with *S*. In order to investigate the correlation, the axial evolution of the normalized $1/COV_{RC}$ is plotted together with the variation of normalized *S* versus $L/D]_H$ downstream of the elbow in Fig. 16. In the figure, both the parameters are normalized by their values at the reference point $L/D]_H$=0, and plotted on the primary and secondary y-axis with logarithmic scales. It is observed that both normalized $1/COV_{RC}$ and *S*, show an approximately one-to-one relationship in the elbow region. Therefore they are correlated by the following equation:

$$\frac{COV_{RC,0}}{COV_{RC}} = C_{rc}\frac{S}{S_0} \tag{16}$$

Here, the coefficient C_{rc} is a constant which can be determined experimentally. By fitting the correlation with experimental data as shown in Fig. 17, it is found that C_{rc}=0.85 predicts the experimental data well for all flow conditions with an average percent difference of less than ±9%.

3.2.4. Modeling of two-phase pressure loss across the elbow

The last term to model in Eq. (1) is the two-phase pressure loss across the elbow. In the straight channel sections, two-phase pressure drop can be predicted reasonably well by the conventional Lockhart–Martinelli correlation (Chisholm, 1967). In two-phase flow through a channel with flow restriction, however, additional pressure loss stemming from the restriction needs to be considered, and the conventional Lockhart–Martinelli correlation is not applicable. To consider restriction effects, Kim et al. (2010) assumes the minor loss mainly comes from the liquid phase in bubbly flow

freepaper.me FREE paper

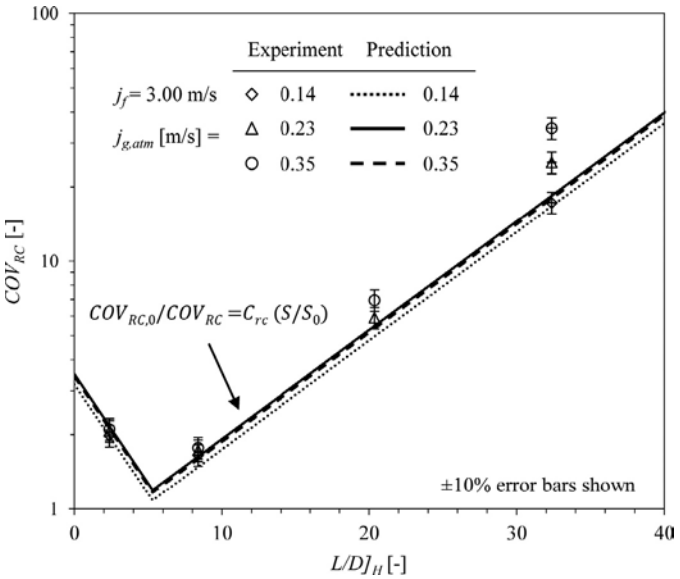

Fig. 17. Prediction of the COV_{RC} in the downstream of the vertical-upward elbow for flow conditions with constant j_f = 3.00 m/s and increasing $j_{g,atm}$.

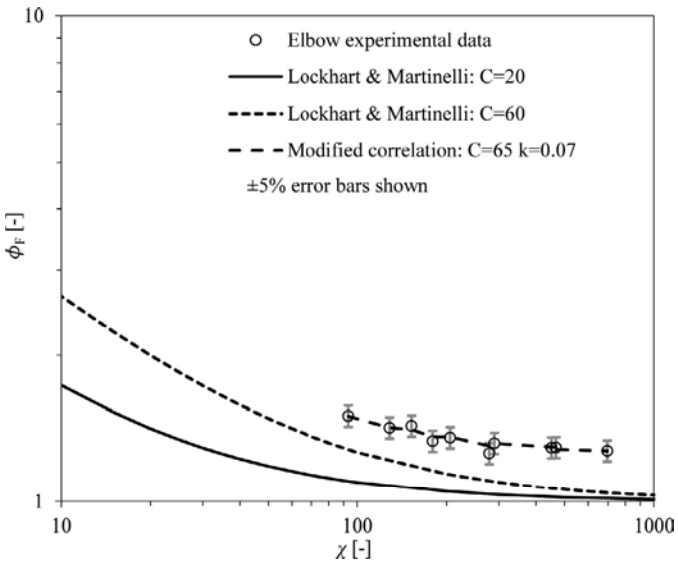

Fig. 18. Comparison of two-phase pressure drop across the vertical-upward elbow with predictions by Lockhart–Martinelli correlation and modified correlation.

and adds an additional minor loss term (stemming from the restriction) to the existing frictional pressure loss terms as shown in Eq. (17).

$$\left(\frac{dp}{dz}\right)_{Total}^{2\phi} = \left(\frac{dp}{dz}\right)_{F}^{2\phi} + \left(\frac{dp}{dz}\right)_{M}^{2\phi} \tag{17}$$

Dividing Eq. (17) by the single-phase liquid pressure drop yields a familiar equation as Lockhart–Martinelli correlation with additional considerations of the minor loss stemming from the flow restriction as given in Eq. (18).

$$\phi_F^2 = \left(1 + \frac{1}{\chi_M^2}\right) + \left(1 + \frac{1}{\chi_M^2}\right)^{1/2} \frac{C}{\chi} + \frac{1}{\chi^2} \tag{18}$$

Here, the two-phase multiplier ϕ_F^2 and the Lockhart–Martinelli parameter χ are defined the same as in single-phase flow. The new parameter χ_M^2 as defined in Eq. (19), on the other hand, reflects the contribution from the flow restriction.

$$\phi_F^2 \equiv \frac{(dp/dz)_{Total}^{2\phi}}{(dp/dz)_F^f}, \quad \chi^2 \equiv \frac{(dp/dz)_F^f}{(dp/dz)_F^g},$$
$$\chi_M^2 \equiv \frac{(dp/dz)_F^f}{(dp/dz)_M^f} = 4\left(\frac{f}{k}\right)\left(\frac{L}{D}\right)_{elbow} \tag{19}$$

In equations above, $(L/D)_{elbow}$ is specified by the elbow geometry as manufactured. The frictional pressure drop due to the ith phase can be obtained using the Fanning equation:

$$\left(\frac{dp}{dz}\right)_F^i = \frac{2f}{D}\rho_i j_i^2, \text{ where } i = f \text{ or } g \tag{20}$$

and the friction factor can be obtained with the Blasius formulation given by:

$$f = m\mathrm{Re}^{-n}, \ \mathrm{Re} = \frac{\rho_i j_i D}{\mu_i},$$
$$\text{with } m = 0.079 \text{ and } n = 0.25 \text{ for turbulent flow} \tag{21}$$

In the modified correlation above, the values for the parameter C and the minor loss factor k need to be determined. According to Kim et al. (2010), the parameter C accounts for the effect of two-phase mixture. They recommend a C value of 65 for both 90° and 45° elbows. The k factor, depending on the types of the flow restriction, is varied to find the best fit to the experimental data. For the current 90° vertical-upward elbow, a k value of 0.07 yields the best fit to the experimental data with an average relative difference of less than ±1.0 % as shown in Fig. 18.

3.2. Model assessment

With the developed predictive models for the bubble velocity advection term, bubble interaction terms, and two-phase pressure loss term, the steady-state one-group IATE in the elbow region is closed. The closed model in the elbow region together with the available models in the vertical-upward and horizontal channels can be implemented to predict $\langle a_i \rangle$ transport in vertical-upward-to-horizontal two-phase flow. However, implementation of IATE models still requires the specification of coefficients for the bubble interaction terms. These coefficients, including C_{TI}, We_{cr}, C_{RC} and α_{max}, are determined and tabulated in Table 3. In the table, all the coefficients except C_{RC} in the transition region and C_{TI} inside the elbow are picked from the previous studies by Ishii et al., (2002, 2004) and Talley (2012). The coefficient C_{RC} in the transition region (bolded in the table) is increased to be 20 times of the value in the vertical-upward section to consider the elbow effects. The coefficient C_{TI} inside the elbow is based on the vertical-downward model (Ishii et al., 2004).

With the discussion above, the developed steady-state one-group IATE and the coefficients are implemented to predict the two-phase flow parameters and to evaluate the developed model. To achieve this, a MATLAB code using a forward difference scheme is written to predict $\langle a_i \rangle$ transport defined by Eq. (1) in the vertical-upward-to-horizontal two-phase flow. At the vertical-upward section, experimental data at port P2 which is located in the middle of the vertical section as shown in Fig. 1 is chosen to provide the inlet conditions for the developed MATLAB code. Flow conditions at port P1 are not selected because two-phase flow is not developed and shows inlet effects here. Then the code calculates the two-phase flow parameters from port P2 until the end of the horizontal section. Detail examples of the IATE code can be found from Yadav (2013).

To evaluate the accuracy of the developed steady-state one-group IATE model, the predicted results are compared with the experimental data. Fig. 19 shows the prediction of $\langle a_i \rangle$ for Run 7

freepaper.me FREE paper

Table 3
One-group IATE coefficients in different regions of the test section.

Mechanisms	Vertical-upward region (Ishii et al., 2002)	Elbow region			Horizontal region (Talley, 2012)
		90° elbow	Transition region	Dissipation region	
TI (source) *RC* (sink)	0.085 ($We_{cr}=6$)	0.085 ($We_{cr}=6$)	0.085 ($We_{cr}=6$)	0.085 ($We_{cr}=6$)	0.014 ($We_{cr}=5$)
$C = 3.0$ $\alpha_{max} = 0.75$	0.004	0.004	**0.08**	0.004	0.003
WE (sink)	0.002	0.002	N/A	N/A	N/A

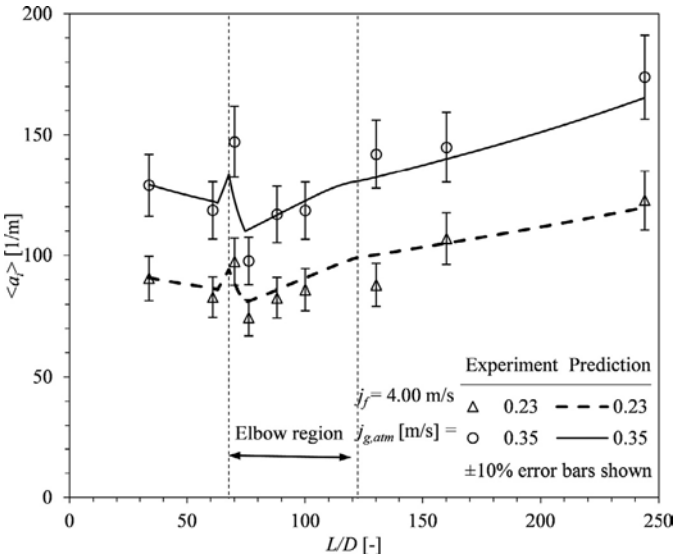

Fig. 19. Predictions of $\langle a_i \rangle$ transport in the vertical-upward-to-horizontal two-phase flow with modified IATE model for Run7 and Run8 ($j_f = 4.00$ m/s, $j_{g,atm} = 0.23$ m/s and 0.35 m/s).

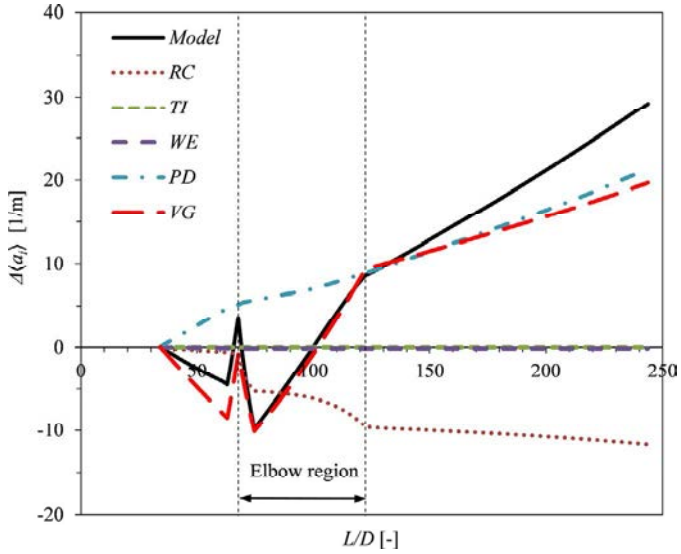

Fig. 20. Individual contributions to $\langle a_i \rangle$ along vertical-to-horizontal section with modified IATE model for Run7 ($j_f = 4.00$ m/s, $j_{g,atm} = 0.23$ m/s).

and Run 8 from the vertical-upward section to the horizontal section. In the figure, the vertical dashed lines represent the elbow region. The horizontal axis *L/D* denotes the distance from the inlet A. It is found that the predictions using the modified IATE model are in good agreement with the experimental data with an average percent difference of less than ±6% throughout the test section. Furthermore, the model provides a good prediction of $\langle a_i \rangle$ at the inlet and the exit of the elbow as well as at the end of the horizontal section. This confirms that the developed model is capable of predicting $\langle a_i \rangle$ from vertical-upward-to-horizontal bubbly flow.

The individual contributions to $\langle a_i \rangle$ transport due to each source/sink term in Eq. (1) for Run 7 are shown in Fig. 20. It is observed that pressure drop (*PD*) term and *RC* term are the source and sink to $\langle a_i \rangle$ throughout the test sections, respectively. The velocity gradient (*VG*)/advection term is a sink to $\langle a_i \rangle$ in the vertical-upward section and then changes to a source to $\langle a_i \rangle$ in the elbow region and remains as a source in the horizontal section. The *TI* term and *WE* term show no contribution in the elbow and horizontal section as they are negligible and not modeled. The change in $\langle a_i \rangle$ across the elbow is primarily governed by the advection term, which is also the dominant source term in the entire elbow region. Since $\langle \langle v_g \rangle \rangle$ is a strong function of the bubble distribution, the drastic change in $\langle \langle v_g \rangle \rangle$ is expected to be caused by the large change in bubble distribution across the elbow. The axial gradient in $\langle \langle v_g \rangle \rangle$, in turn acts as source/sink to $\langle a_i \rangle$. Another point is random collision is a large sink to $\langle a_i \rangle$ in the transition region which can be explained by the secondary flow promoting bubble collision.

Fig. 21 shows the prediction of $\langle a_i \rangle$ transport for Run5 from the vertical-upward section to the horizontal section. Overall, good

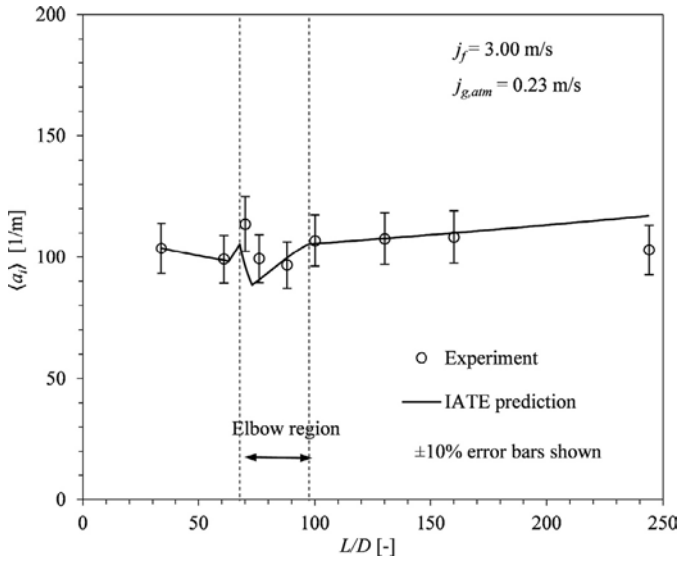

Fig. 21. Predictions of $\langle a_i \rangle$ transport in the vertical-upward-to-horizontal two-phase flow with modified IATE model for Run5 ($j_f = 3.00$ m/s, $j_{g,atm} = 0.23$ m/s).

agreement of $\langle a_i \rangle$ prediction with an average percent difference of less than ±6% compared with experimental data is observed. However, it should be noted that the model predicts an increasing trend between $L/D = 161$ and 244 while the experimental data show an opposite decreasing trend. This is because Run5 is not a purely bubbly flow condition in the downstream of the elbow and large group-II bubbles (slug or plug bubbles) are observed between

freepaper.me FREE paper

L/D = 161 and 244, as indicated in Fig. 8. As a result, experimental data show a decreasing trend in $\langle a_i \rangle$ between L/D =161 and 244. This demonstrates that the current model works for the bubbly flow condition but may not work at further downstream of the elbow where the group-II bubbles start to appear. This also shows the significance of developing a two-group IATE model in the presence of flow restrictions such as elbows.

4. Summary and conclusions

The current study extends the experimental database established by Yadav et al. (2014a, b) by acquiring additional experimental data near the exit of the 90° vertical-upward elbow. With the newly acquired data, two-phase flow parameters downstream of the elbow can be normalized to facilitate the development of new models. Also, new database shows that the vertical-upward elbow has similar restriction effects on development of the bubble distribution for all two-phase flow conditions performed in the experiment. In general, there exist three characteristic regions in void distribution, including a bimodal-to-bimodal region, a bimodal-to-single-peaked region, and a developed horizontal flow region with void accumulated at the top of the pipe cross-section. The detailed database can also be used to develop and benchmark multiphase flow CFD.

With the new database, the predictive model for elbow dissipation length is modified by including the transition region in addition to the existing dissipation region. Then, bubble velocity advection term and covariance in bubble interaction terms are correlated with the *elbow-strength, S*. The two-phase frictional pressure drop across the elbow is modeled using the modified Lockhart–Martinelli correlation by Kim et al., (2010). The IATE predictive model is closed by combining all the developed models above.

The developed model in the elbow region together with the available models in the vertical-upward and horizontal channels are implemented to predict $\langle a_i \rangle$ transport in the vertical-upward-to-horizontal two-phase flow. Coefficients for the bubble interaction terms including C_{TI}, We_{cr}, C_{RC} and α_{max} are determined from the previous studies. The coefficient C_{RC} in the transition region is increased to be 20 times of the value in the vertical-upward section to reflect the effect of secondary flow that significantly promotes bubble coalescence. The developed IATE model is evaluated by comparing the predicted results with the experimental data. In general, the developed IATE model is capable of predicting $\langle a_i \rangle$ transport from vertical-upward-to-horizontal bubbly flow with an average percent difference of less than ±6%. In flow conditions where group-II bubbles form far downstream of the elbow, the prediction starts to deviate as expected. In such conditions, a two-group IATE model in the elbow region is required.

References

Chisholm, D., 1967. A theoretical basis for the Lockhart-Martinelli correlation for two-phase flow. Int. J. Heat Mass Transf. 10, 1767–1778.

Hibiki, T., Ishii, M., 2000. One-group interfacial area transport of bubbly flows in vertical round tubes. Int. J. Heat Mass Transf. 43, 2711–2726.

Ishii, M., 1975. Thermo-Fluid Dynamic Theory of Two-phase Flow. Collection de la Direction des Etudes et Recherches d'Electricite de France, Eyrolles.

Ishii, M., Kim, S., Uhle, J., 2002. Interfacial area transport equation: Model development and benchmark experiments. Int. J. Heat Mass Transf. 45, 3111–3123.

Ishii, M., Paranjape, S.S., Kim, S., Sun, X., 2004. Interfacial structures and interfacial area transport in downward two-phase bubbly flow. Int. J. Multiph. Flow 30, 779–801.

Kataoka, I., Ishii, M., Serizawa, A., 1986. Local formulation and measurements of interfacial area concentration in two-phase flow. Int. J. Multiph. Flow 12, 505–529.

Kim, S., 1999. Interfacial area Transport Equation and Measurement of Local Interfacial Characteristics. Purdue University.

Kim, S., Fu, X.Y., Wang, X., Ishii, M., 2000. Development of the miniaturized four-sensor conductivity probe and the signal processing scheme. Int. J. Heat Mass Transf. 43 (22), 4101–4118.

Kim, S., Kojasoy, G., Guo, T., 2010. Two-phase minor loss in horizontal bubbly flow with elbows: 45° and 90° elbows. Nucl. Eng. Des. 240, 284–289.

Kim, S., Park, J.H., Kojasoy, G., Kelly, J.M., Marshall, S.O., 2007. Geometric effects of 90-degree elbow in the development of interfacial structures in horizontal bubbly flow. Nucl. Eng. Des. 237, 2105–2113.

Lucas, D., Beyer, M., Kussin, J., Schütz, P., 2010. Benchmark database on the evolution of two-phase flows in a vertical pipe. Nucl. Eng. Des. 240, 2338–2346.

Qiao, S., Mena, D., Kim, S., 2016. Inlet effects on vertical-downward air-water two-phase flow. Nucl. Eng. Des. in press, doi:10.1016/j.nucengdes.2016.04.033.

Salcudean, M., Groeneveld, D.C., Leung, L., 1983. Effect of flow-obstruction geometry on pressure drops in horizontal air-water flow. Int. J. Multiph. Flow 9, 73–85.

Taitel, Y., Duckler, A.E., 1976. A model for predicting flow regime transitions in horizontal and near horizontal gas-liquid flow. AIChE J 22 (1), 47–55.

Talley, J., Kim, S., Guo, T., Kojasoy, G., 2009. Geometric effects of 45-deg elbow in horizontal air-water bubbly flow. Nucl. Technol. 167, 2–12.

Talley, J.D., 2012. Interfacial Area Transport Equation for Vertical and Horizontal Bubbly Flows and its Application to the Trace Code. The Pennsylvania State University.

Wang, C.C., Chen, I.Y., Yang, Y.W., Hu, R., 2004. Influence of horizontal return bend on the two-phase flow pattern in small diameter tubes. Exp. Therm. Fluid Sci. 28, 145–152.

Wheeler, J., Rau, A., Worosz, T., Kim, S., 2014. Experimental investigation on the effects of a spacer grid on single- and two-phase flows. Int. J. Nucl. Energy Sci. Eng. 4, 50.

Wu, Q., Ishii, M., 1999. Sensitivity study on double-sensor conductivity probe for the measurement of interfacial area concentration in bubbly flow. Int. J. Multiph. Flow 25, 155–173.

Wu, Q., Kim, S., Ishii, M., Beus, S.G., 1998. One-group interfacial area transport in vertical bubbly flow. Int. J. Heat Mass Transf. 41, 1103–1112.

Yadav, M.S., 2013. Interfacial Area Transport Across Vertical Elbows in Air-Water Two-phase Flow. The Pennsylvania State University.

Yadav, M.S., Kim, S., Tien, K., Bajorek, S.M., 2014a. Experiments on geometric effects of 90-degree vertical-upward elbow in air water two-phase flow. Int. J. Multiph. Flow 65, 98–107.

Yadav, M.S., Worosz, T., Kim, S., Tien, K., Bajorek, S.M., 2014b. Characterization of the dissipation of elbow effects in bubbly two-phase flows. Int. J. Multiph. Flow 66, 101–109.

freepaper.me FREE paper